A Unique Combination of Equatorial Plasma Bubble Morphologies Occurring Within a 12^{o} Longitude Range

Deepak Kumar Karan[1], Richard W. Eastes[1], Carlos R. Martinis[2], Robert E. Daniell[3], Stanley C. Solomon[4] and William E. McClintock[1]

[1]Laboratory for Atmospheric and Space Physics, University of Colorado, Boulder, CO, USA
[2]Center for Space Physics, Boston University, MA, USA
[3]Ionospheric Physics, Stoughton, MA, USA
[4]High Altitude Observatory, National Center for Atmospheric Research, Boulder, CO, USA

Corresponding author: Deepak Kumar Karan (Deepak.Karan@lasp.colorado.edu)

Key Points:

- First simultaneous observations of C-shape, straight, and reversed C-shape EPBs within 12^{o} longitude range
- Observations indicate longitudinal variations in EPBs' zonal drift velocities at the magnetic equator and EIA crests
- Different EPBs' shapes in such short longitudes point to small-scale gradients in neutral winds or electric field effects

Key Words: NASA GOLD mission, Equatorial Plasma Bubbles, EPB Morphology, Plasma Irregularities, Nighttime ionosphere, OI 135.6 nm nightglow

Abstract:

On 12 October 2020, the NASA's Global-scale Observations of the Limb and Disk (GOLD) mission observed three differently shaped EPBs within a 12^{o} longitude range, near the subsatellite point. One is straight aligned to the magnetic field line, whereas the poleward extensions of the others are tilted eastward and westward from the magnetic field line resembling a C-shape and reversed C-shape structures. These EPBs were inside the GOLD imager's field-of-view for a period of ~3 hours. This allowed us to compute their zonal motion and determine their drift velocities. EPBs' drift velocities were derived from measuring their longitudinal shifts at the magnetic equator and at both EIA crests. This unique observation, showing three morphologies in a narrow longitude sector, indicates the occurrence of strong longitudinal gradients in the typical parameters associated with the dynamics of EPBs, like neutral winds, electric fields, or other parameters within such a narrow longitude range.

Plain Language Summary:

The post-sunset ionosphere becomes conducive to the formation of plasma irregularities that are associated with depleted plasma densities. In the images obtained from space or ground, these plasma depleted regions appear as latitudinally elongated dark bands, which are known as "equatorial plasma bubbles (EPBs)". The trans-ionospheric radio wave propagation, satellite communication, and navigation systems are adversely affected while the signals travel through the EPBs. Thus, investigations of EPBs' formation and development are important. On 12 October 2020, the NASA's Global-scale Observations of the Limb and Disk (GOLD) mission observed the three differently shaped EPBs within a 12^{o} longitude range, near the subsatellite point. One is straight aligned to the magnetic field line, whereas the poleward extensions of the others are tilted eastward or westward from the magnetic field line resembling a C-shape or reversed C-shape structure. This is the only observation of this kind so far reported to the best of our knowledge. Such observation indicates the occurrence of strong longitudinal gradients in neutral winds or electric fields. We are presenting detailed information on the observations, obtained their zonal drift velocities at different latitudes, and discussed the possible explanation of their occurrences.

Introduction:

Equatorial plasma bubbles (EPBs), a nighttime plasma irregularity phenomenon, occur within the equatorial and low-latitude ionosphere. Trans-ionospheric radio wave propagation for communication, navigation, and timing is adversely affected when passing through the plasma irregularities in this region. Thus, the investigation of plasma irregularities is an important priority for researchers, with societal implications. The formation and development of EPBs depend on several factors such as vertical and horizontal ionospheric density gradient (both neutral and plasma), background neutral winds, zonal electric fields, chemical recombination, and atmospheric waves (Sultan, 1996; Taori et al., 2011; Liu et al., 2017; Bhattacharyya, 2022). EPBs are expected to be aligned to the magnetic field lines, and in 2-D airglow images, they appear to be straight. However, in different cases, the poleward extensions of the EPBs are observed to be tilted eastward or westward from the magnetic field line resembling either a C-shape or reversed C-shape structures, respectively.

Using a ground-based all-sky airglow imaging system, westward skewness of the airglow depletions with respect to the magnetic field line away from the magnetic equator was reported (Mendilo and Baumgardner, 1982; Mendilo and Tyler, 1983). A decrease of the eastward plasma drift velocity with increasing altitude (latitude) could be produced if the eastward neutral wind velocity also decreases with altitude (latitude), a direct consequence of a fully working F-region dynamo (Rishbeth, 1972). This latitudinal gradient in the zonal neutral wind has been observed by Dynamics Explorer-2 satellite (Raghavarao et al., 1991) and ground-based Fabry-Perot interferometer (Martinis et al., 2001, 2003). Reversed C-shape EPB was observed in the OI 135.6-nm emission images by the Global Ultraviolet Imager (GUVI) on board the Thermosphere, Ionosphere, Mesosphere Energetics and Dynamics (TIMED) satellite (Kelley et al., 2003). The vertical shear in the eastward plasma flow velocity, which peaks near the F peak at the magnetic equator is attributed to the formation of the EPB structure. Kil et al., (2009) proposed a shell structure to understand this reversed C-shape structure. Several 2-D and 3-D simulation efforts have been put forward in this regard (Huba et al., 2009, 2020; Yokoyama, 2017 and references therein).

On October 12, 2020, the NASA Global-scale Observations of the Limb and Disk (GOLD) mission observed three EPBs; a C-shape, a straight, and a reversed C-shape EPB occurring within 12^{o} of longitude near the subsatellite point (~47^{o} W). Such occurrence of three consecutive different structured EPBs has not been observed before. This paper reports the observations of this rare event with a discussion about the possible causes of its occurrence.

Data:

Nighttime OI 135.6 nm partial disk scans made by the GOLD imager are the primary data sets used in this study. The GOLD imager was launched on 25 January 2018 and is located in geostationary orbit at 47.5^{o}W, carried on a commercial communications satellite. Nominal operations and observations started on 9 October 2018. It has two identical spectrographs that obtain images of the Earth in the far-ultraviolet (FUV) range, at ~132-162 nm wavelength. It measures the column integrated emission rate along the line of sight. The night time peak emission altitude for OI 135.6 nm is considered to be at 300 km when geolocating the pixels. GOLD is able to observe the American, Atlantic, and Western African longitudinal regions, which provides a unique opportunity to unambiguously observe the spatial-temporal evolution of various ionospheric-thermospheric features in this active region of the Equatorial Ionization Anomaly (EIA). The night time L1C disk images are obtained at a cadence of 15 minutes and binned to a spatial resolution of 96×80 km at the nadir. Detailed information about the GOLD instrument, observation mode, and data products with some initial observations are discussed in Eastes et al., (2017, 2020) and McClintock et al., (2020).

Results and Discussion:

GOLD takes nighttime disk observations using both channels A and B (CHA and CHB hereafter). Most individual scans cover ~45° in longitude, ~3 hours in local time, just east of the sunset terminator. Starting from 20:10 UT, CHB takes the night time partial disk images alternating between the Northern and Southern hemispheres. Simultaneous observations from the Northern and Southern hemispheres are made from 23:10 to 00:09 UT, using CHA and CHB. The observation sequence is described in detail by Karan, et al. (2020). On 12 October 2020 GOLD measured three closely spaced EPBs during 23:10 and 23:55 UT. Figure 1 shows simultaneous

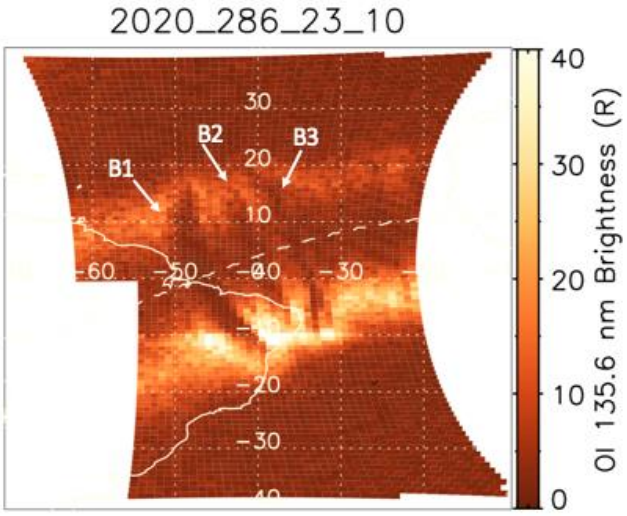

Figure 1. The nighttime images obtained by GOLD in OI 135.6 nm simultaneously by CHA and CHB at 23:10 UT on 12 October 2020 are combined. The white dashed line shows the geomagnetic equator. The two bright emission patches seen at all longitudes on either side of the magnetic equator are the EIA crests. Depletions in the brightness across the EIA crests, known as Equatorial Plasma Bubbles (EPBs), are seen. The C-shape, straight, and reversed C-shape EPBs are noted as B1, B2, and B3, respectively.

images obtained by CHA and CHB from the northern and southern hemispheres at 23:10 UT. The white dashed line shows the geomagnetic equator. The observed bright emissions on either side of the geomagnetic equator are the EIA crests. The horizontal glitch in brightness at 10ºS GLat is a data artifact due to the high voltage being too low during the flat field measurements, which is explained in section 3.1.18 of the GOLD data release note Rev 4.6 (https://gold.cs.ucf.edu/wp-content/documentation/GOLD_Release_Notes_Rev4.6.pdf). Depletions in the brightness across the EIA crests are identified as EPBs. Three clear and distinct EPBs over the Eastern side of South America are observed in this image. The EPB on the left side (marked as B1) has a C-shape structure, the one in the middle (marked as B2) is almost straight, whereas the right EPB (marked as B3) has a reversed C-shape structure. Each type of EPB structure has been observed in the past, but the observations on October 12, 2020, represent a rare event where the three different types of EPBs occur consecutively over a narrow longitude range (~12º) between ~47º W and 35.5º W. This longitude range is close to the crossing longitude of geographic and geomagnetic equators, and also near to the subsatellite location of the GOLD imager.

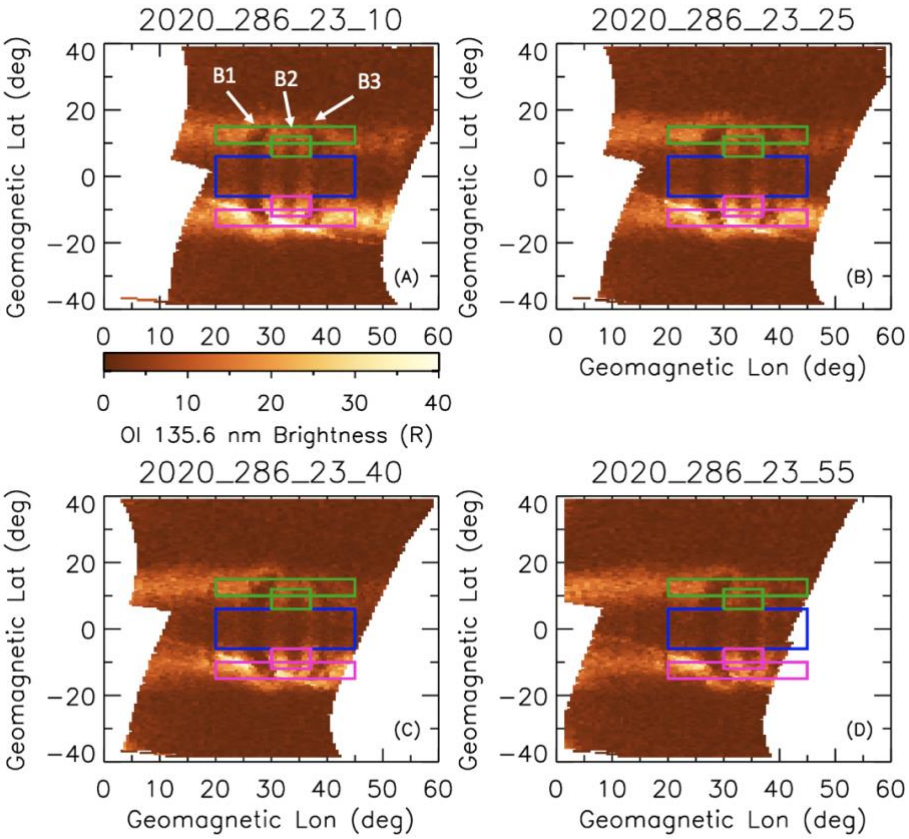

Figure 2. (A, B, C, and D) show the nighttime images observed by GOLD at 23:10, 23:25, 23:40, and 23:55 UT, respectively in geomagnetic co-ordinates. The green, blue, and magenta boxes are the regions selected at the N- crest, magnetic equator, and S- crest of EIA latitudes (common on each panel).

In order to investigate the different shapes of these EPBs within the narrow longitude range in detail, we transformed the EPBs from geographic coordinates into QD dipolar magnetic co-ordinates (Laundal and Richmond, 2017; Thébault et al., 2015). Figures 2 (A), (B), (C), and (D) show the nighttime images observed by GOLD at 23:10, 23:25, 23:40, and 23:55 UT, respectively in magnetic coordinates. At 23:10 UT (Figure 2A) the locations of B1, B2, and B3 at the magnetic equator are (47^{o} W Glon, 0.5^{o} N Glat, 26.5^{o} Mlon), (40^{o} W Glon, 2.5^{o} N Glat, 33.2^{o} Mlon), and (35.5^{o} W Glon, 5.7^{o} N Glat, 38.5^{o} Mlon), respectively. We next investigated their zonal motion (or shifts) at different magnetic latitude ranges. We selected three magnetic latitude regions, (10^{o} to 15^{o}), (-6^{o} to 6^{o}), and (-15^{o} to -10^{o}), shown by green, blue, and magenta boxes, respectively, in Figure 2. The latitude ranges are selected to distinguish both the EIA crests from the magnetic equatorial region. The green and magenta boxes cover the N and S EIA crests latitudes. The blue

boxes cover the magnetic equatorial latitudes. We note that B2 reaches lower latitudes than B1 and B3. So, for B2 the selected magnetic latitude ranges at EIA crests are (6^o to 12^o) and (-12^o to -6^o). The brightness along the latitudes in each box are summed at each longitude. From the longitudinal variations of the summed brightness, the longitudes of the EPBs are obtained. This method of obtaining the EPB location is explained in detail by Karan et al., 2020. Longitudes of B1, B2, and B3 at the three latitude ranges are obtained from the partial disk images covering the EPBs on October 12, 2020. The obtained EPB locations at the different latitude ranges are shown in Figure 3.

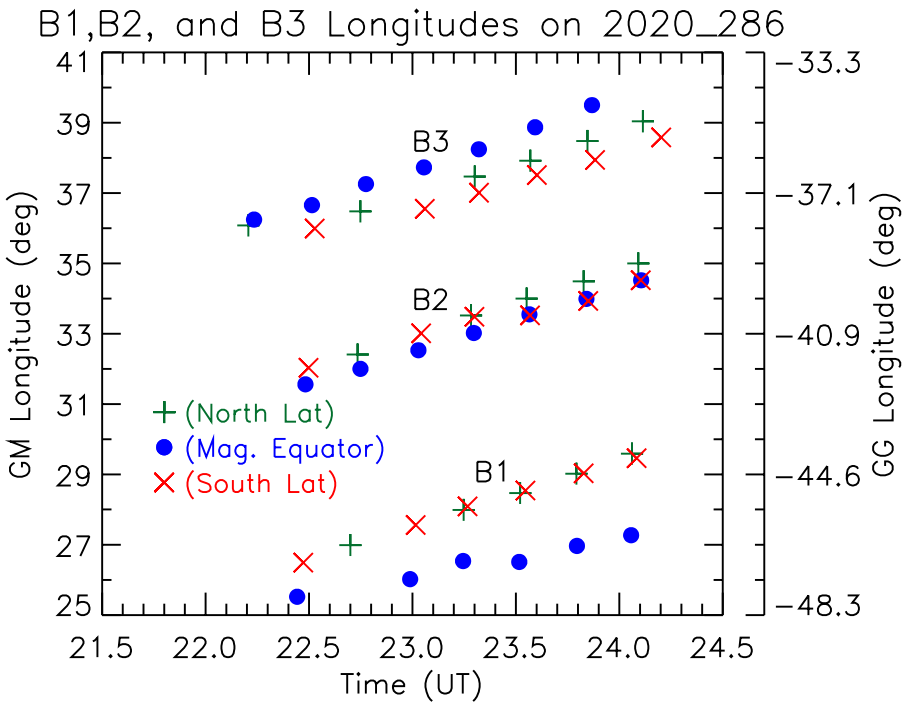

Figure 3 shows EPB (B1, B2, and B3) longitudes at different times of observations. Blue dot, green plus, and red cross symbols indicate to longitudes as obtained at the magnetic equator, N and S EIA crests latitudes, respectively.

Longitudes of each EPB are obtained at the magnetic equator, N and S EIA crests latitudes, which are shown by blue dots, green plus, and red cross symbols, respectively in figure 3. The EPB locations are obtained multiple times, one of the advantages of the GOLD observations. Earlier detection of B3 at 22:10 UT is due to the GOLD imager's observation sequence from east to west following the sunset terminator. EPBs are developed at the geomagnetic equator and grow to

higher altitudes and latitudes. Thus, EPBs are detected first closer to equatorial latitudes. One common pattern observed is that three EPBs shift to east longitudes with time at each latitude range. From the temporal shifts of the locations, EPB drift velocities can be derived. Using the method discussed in Karan et al. (2020), drift velocities of B1, B2, and B3 are obtained at the three latitude ranges and are listed in the table.

Magnetic Latitude Zone	B1 (C-shape)	B2 (Straight)	B3 (reversed C-shape)
N-EIA crest	65 ± 2	62 ± 4	57 ± 9
Equator	48 ± 6	62 ± 2	68 ± 4
S-EIA crest	62 ± 3	61 ± 5	52 ± 5

Table 1. Zonal drift velocities (m/s) of B1, B2, and B3 at the magnetic equator, N and S EIA crest latitudes

The drift velocities of B1 are 65 ± 2, 48 ± 6, and 62 ± 3 m/s at the N crest, magnetic equator, and S crest, respectively. At the EIA crest latitudes, B1 was drifting faster than at the equator. This can explain its C-shape structure. B2 was drifting at a constant velocity of ~62 m/s at all the latitude ranges. As a result, it had a straight shape, not showing any latitudinal variation. The drift velocities of B3 are 57 ± 9, 68 ± 4, and 52 ± 5 m/s at the N crest, magnetic equator, and S crest, respectively. B3 was drifting faster near the magnetic equator than at the EIA crest latitudes. This resulted in the reversed C-shape B3. The obtained EPB drift velocities explain the observed different EPB structures.

All these differences were observed in a short longitude range of ~12 degrees. As explained earlier, the behavior of zonal winds affects the motion of plasma drifts, thus we can interpret the shapes observed as a consequence of the varying conditions on the thermospheric neutral winds at these longitudes. Geomagnetic conditions were quiet during this time, so we can exclude any storm effects. We would expect larger ion drag forces to reduce the neutral zonal wind speeds at the EIA crests, allowing faster winds at the magnetic equator. As a result, EPB zonal drift velocity would be reduced at these crest latitudes (Raghavarao et al., 1991; Martinis et al., 2001, 2003; Valladares et al., 2002) and a reversed C-shape structure would be formed. This is the case with B3. Since B2 did not evolve to latitudes reaching the peak of the EIA crests, ion drag effects might not be too

different at the N and S crests when compared to the magnetic equator. As a consequence, the EPB drift velocities observed would be similar, and no latitudinal variation in the shape of B2 is observed. However, the ion drag force mechanism does not explain the formation of the C-shape EPB B1 where the drift velocities at the EIA crests are faster than at the equator. A way to reduce a thermospheric neutral wind is through the presence of significant E region contribution to ionization. That would preclude a full F region dynamo operating at the equatorial and low latitudes. As a consequence, the drifts would be slower when compared to the ones observed at higher latitudes, near the peak of the EIA crests, where E-region effects would not be as strong. Thus, while we expect ion drag still affect the overall motion of plasma, E region effects are stronger at the magnetic equator. In fact, from Table 1 we can see that the drifts at the magnetic equator are smallest for B1. Small spatial scale variations (~3^{o} longitude) in the equatorial electric fields have been reported by Karan and Pallamraju (2017).

Conclusions:

We have reported a rare occurrence of the EPB morphology using the NASA's GOLD mission observations. Three consecutive EPBs with C-shape, straight, and reversed C-shape structures are observed within a 12^{o} longitude range over the eastern side of South America on October 12, 2020. The longitude of observation of this event is close to the crossing of geographic and geomagnetic equators and also, close to the subsatellite point of the GOLD imager. The drift velocities of B1, B2, and B3 at three latitudes are given in Table 1. Latitudinal variations in drift velocities can explain the difference EPBs' shapes. Different EPBs' shapes in such short longitude range point to small scale gradients in neutral winds or E-region effects at earlier local times.

Acknowledgements:

This research is supported by NASA contract 80GSFC18C0061 to the University of Colorado.

Open Research:

The GOLD L1C nighttime partial disk data presented in this paper (Level 1C – NI1) can be accessed at the GOLD Science Data Center (http://gold.cs.ucf.edu/search/). Please be sure to read the GOLD data release note Rev 4.6 (https://gold.cs.ucf.edu/wp-content/documentation/GOLD_Release_Notes_Rev4.6.pdf).

Reference:

Bhattacharyya, A. (2022). Equatorial Plasma Bubbles: A Review. Atmosphere 2022, 13, 1637. https://doi.org/10.3390/atmos13101637

Eastes, R. W., McClintock, W. E., Burns, A. G., Anderson, D. N., Andersson, L., Codrescu, M., et al. (2017). The Global-scale Observations of the Limb and Disk (GOLD) mission. Space Sci Rev, 212, 383, doi:10.1007/s11214-017-0392-2

Eastes, R. W., McClintock, W. E., Burns, A. G., Anderson, D. N., Andersson, L., Aryal, S., et al. (2020). Initial observations by the GOLD mission. J. Geophys. Res. Space Physics, 125, e2020JA027823, doi:10.1029/2020JA027823

Huba, J. D., S. L. Ossakow, G. Joyce, J. Krall, and S. L. England (2009), Three-dimensional equatorial spread F modeling: Zonal neutral wind effects, Geophys. Res. Lett., 36, L19106, doi:10.1029/2009GL040284.

Huba, J. D., & Liu, H.-L. (2020). Global modeling of equatorial spread F with SAMI3/WACCM-X. Geophysical Research Letters, 47, e2020GL088258. https://doi.org/10.1029/2020GL088258

Karan, D. K., and D. Pallamraju, (2017). Small-scale longitudinal variations in the daytime equatorial thermospheric wave dynamics as inferred from oxygen dayglow emissions. J. Geophys. Res. Space Physics, 122, 6528-6542, doi:10.1002/2017JA023891

Karan, D. K., Daniell, R. E., England, S. L., Martinis, C. R., Eastes, R. W., Burns, A. G., & McClintock, W. E. (2020). First zonal drift velocity measurement of equatorial plasma bubbles (EPBs) from a geostationary orbit using GOLD data. J. Geophys. Res. Space Physics, 125, e2020JA028173, doi:10.1029/2020JA028173

Kelley, M. C., Makela, J. J., Paxton, L. J., Kamalabadi, F., Comberiate, J. M., and Kil, H. (2003), The first coordinated ground- and space-based optical observations of equatorial plasma bubbles, Geophys. Res. Lett., 30, 1766, doi:10.1029/2003GL017301, 14.

Kil, H., R. A. Heelis, L. J. Paxton, and S.-J. Oh (2009), Formation of a plasma depletion shell in the equatorial ionosphere, J. Geophys. Res., 114, A11302, doi:10.1029/2009JA014369.

Laundal, K. M., and Richmond, A. D. (2017) Magnetic Coordinate Systems, Space Sci Rev, 206, 27-59. https://doi.org/10.1007/s11214-016-0275-y

Liu, H., N. Pedatella, and K. Hocke (2017), Medium-scale gravity wave activity in the bottomside F region in tropical regions, Geophys. Res. Lett., 44, 7099–7105, doi:10.1002/2017GL073855.

Martinis, C., J. Meriwether, M. Biondi, R. Niciewjewski, C. Fesen, and M. Mendillo (2001), Zonal neutral winds at equatorial and low-latitudes, J. Atmos. Sol. Terr. Phys., 63, 1559–1569.

Martinis, C., Eccles, J. V., Baumgardner, J., Manzano, J., & Mendillo, M. (2003). Latitude dependence of zonal plasma drifts obtained from dual-site airglow observations. Journal of Geophysical Research, 108(A3), 1129. https://doi.org/10.1029/2002JA009462

McClintock, W. E., Eastes, R. W., Beland, S., Bryant, K. B., Burns, A. G., Correira, J., et al (2020). Global-scale Measurements of the Limb and Disk (GOLD) Mission Implementation: 2. Observations, Data Pipeline and Level 1 Data Products. Journal of Geophysical Research: Space Physics, 125, e2020JA027809. https://doi.org/10.1029/2020JA027809.

Raghavarao, R., L. E. Wharton, N. W. Spencer, H. G. Mayr, and L. H. Brace (1991), An equatorial temperature and wind anomaly (ETWA), Geophys. Res. Lett., 18 (7), 1193–1196, doi:10.1029/91GL01561.

Richmond, A. D. (1995), Ionospheric electrodynamics using magnetic apex coordinates, J. Geomagn. Geoelectr., 47, 191–212, https://doi.org/10.5636/jgg.47.191.

Rishbeth, H (1972), Thermospheric winds and the F-region: A review, Journal of Atmospheric and Terrestrial Physics, 34, https://doi.org/10.1016/0021-9169(72)90003-7.

Sultan, P. J. (1996), Linear theory and modeling of the Rayleigh-Taylor instability leading to the occurrence of equatorial spread F, J. Geophys. Res., 101(A12), 26875– 26891, doi:10.1029/96JA00682.

Taori, A., A. K. Patra, and L. M. Joshi (2011), Gravity wave seeding of equatorial plasma bubbles: An investigation with simultaneous F region, E region, and middle atmospheric measurements, J. Geophys. Res., 116, A05310, doi:10.1029/2010JA016229.

Thébault, E., Finlay, C.C., Beggan, C.D. et al. (2015), International Geomagnetic Reference Field: the 12th generation. Earth Planet Sp 67, 79, doi:10.1186/s40623-015-0228-9.

Tsunoda, R. T., R. C. Livingston, and C. L. Rino (1981), Evidence of a velocity shear in bulk plasma motion associated with the post-sunset rise of the equatorial F layer, Geophys. Res. Lett., 8, 807–810, doi:10.1029/GL008i007p00807.

Valladares, C. E., J. W. Meriwether, R. Sheehan, and M. A. Biondi, Correlative study of neutral winds and scintillation drifts measured near the magnetic equator, J. Geophys. Res., 107(A7), 1112, doi:10.1029/2001JA000042, 2002.

Yokoyama, T. A review on the numerical simulation of equatorial plasma bubbles toward scintillation evaluation and forecasting. Prog Earth Planet Sci 4, 37 (2017). https://doi.org/10.1186/s40645-017-0153-6